Ain Shams Engineering Journal (2017) 8, 145–162

Ain Shams University

Ain Shams Engineering Journal

www.elsevier.com/locate/asej
www.sciencedirect.com

ENGINEERING PHYSICS AND MATHEMATICS

Mixed convection boundary layer flows of a non-Newtonian Jeffrey's fluid from a non-isothermal wedge

S. Abdul Gaffar [a,*], V. Ramachandra Prasad [b], E. Keshava Reddy [a]

[a] Department of Mathematics, Jawaharlal Nehru Technological University Anantapur, Anantapuramu, India
[b] Department of Mathematics, Madanapalle Institute of Technology and Science, Madanapalle 517325, India

Received 22 May 2015; revised 25 August 2015; accepted 10 September 2015
Available online 17 October 2015

KEYWORDS

Non-Newtonian Jeffrey's fluid model;
Non-isothermal wedge;
Finite difference numerical method;
Boundary layers;
Deborah number

Abstract This article presents the nonlinear, steady state mixed convection boundary layer flow, heat and mass transfer of an incompressible non-Newtonian Jeffrey's fluid past a non-isothermal wedge. The transformed conservation equations are solved numerically subject to physically appropriate boundary conditions using a versatile, implicit finite-difference Keller box technique. The influence of a number of emerging non-dimensional parameters, namely Deborah number (De), ratio of relaxation to retardation times (λ), pressure gradient parameter (m), Buoyancy ratio parameter (N), mixed convection parameter (λ_1), radiation parameter (F) and heat generation/absorption parameter (Δ) on velocity, temperature and concentration evolution in the boundary layer regime is examined in detail. Also, the effects of these parameters on *surface heat transfer rate*, *mass transfer rate* and *local skin friction* are investigated.

1. Introduction

Non-Newtonian transport phenomena arise in many branches of process mechanical, chemical and materials engineering. Most non-Newtonian models involve some form of modification to the momentum conservation equations. These include power-law fluids [1], Walters-B short memory models [2,3], Oldroyd-B models [4], differential Reiner–Rivlin models [5,6], Bingham plastics [7] and tangent hyperbolic fluids [8].

As with a number of rheological models developed, the Jeffrey model has proved quite successful. This simple, yet elegant rheological model was introduced originally to simulate earth crustal flow problems [9]. This model [10] constitutes a viscoelastic fluid model which exhibits shear thinning characteristics, yield stress and high shear viscosity. The Jeffrey fluid model degenerates to a Newtonian fluid at a very high wall shear stress i.e. when the *wall stress is much greater than yield stress*. This fluid model also approximates reasonably well the rheological behavior of other liquids including physiological suspensions, foams, geological materials, cosmetics, and

* Corresponding author.
E-mail addresses: abdulsgaffar0905@gmail.com (S.A. Gaffar), rcpmaths@gmail.com (V.R. Prasad), eddulakr@gmail.com (E. Keshava Reddy).
Peer review under responsibility of Ain Shams University.

Production and hosting by Elsevier

http://dx.doi.org/10.1016/j.asej.2015.09.005

Nomenclature

C	concentration
C_f	skin friction coefficient
c_p	specific heat parameter
De	Deborah number
D_m	mass (species) diffusivity
f	non-dimensional steam function
F	thermal Radiation
$\boldsymbol{g}$	acceleration due to gravity
Gr_x	Grashof (free convection) number
K	thermal diffusivity
k	thermal conductivity of Jeffrey's fluid
k^*	mean absorption coefficient
m	pressure gradient parameter
Nb	buoyancy ratio parameter
Nu	heat transfer rate (local Nusselt number)
Pr	Prandtl number
q_r	radiative heat flux
Re_x	Reynolds number
$\boldsymbol{S}$	Cauchy stress tensor
Sc	local Schmidt number
Sh	mass transfer rate (Sherwood number)
T	temperature of the Jeffrey's fluid
u, v	non-dimensional velocity components along the x- and y-directions, respectively
x	stream wise coordinate
y	transverse coordinate

Greek symbols

α	thermal diffusivity
β	coefficient of thermal expansion
β^*	coefficient of concentration expansion
λ	ratio of relaxation to retardation times
λ_1	mixed convection parameter
λ_2	retardation time
η	dimensionless radial coordinate
μ	dynamic viscosity
ν	kinematic viscosity
θ	non-dimensional temperature
ϕ	non-dimensional concentration
ρ	density of fluid
ξ	dimensionless tangential coordinate
Ψ	dimensionless stream function
Δ	heat generation (source)/heat absorption (sink) parameter
σ^*	Stefan–Boltzmann constant

Subscripts

w	surface conditions on wedge
∞	free stream conditions

syrups. Interesting studies employing this model include peristaltic transport of Jeffery fluid under the effect of magnetohydrodynamic [11], peristaltic flow of Jeffery fluid with variable-viscosity [12], radiative flow of Jeffery fluid in a porous medium with power law heat flux and heat source [13], recent studies on Jeffrey's fluid include [14–16].

The heat transfer analysis of boundary layer flow with radiation is important in various materials processing operations including high temperature plasmas, glass fabrication, and liquid metal fluids. When coupled with thermal convection flows, these transport phenomena problems are highly nonlinear. At a high temperature the presence of thermal radiation changes the distribution of temperature in the boundary layer, which in turn affects the heat transfer at the wall. A number of studies have appeared that consider multi-physical radiative–convective flows. Recently, Asmat Ara et al. [17] reported the radiation effect on boundary layer flow of Eyring-Powell fluid from an exponentially shrinking sheet. Noor et al. [18] used the Rosseland model to study radiation effects on hydromagnetic convection with thermophoresis along an inclined plate. Further, studies employing the Rosseland model include Gupta et al. [19] who examined on radiative convective micropolar shrinking sheet flow, Cortell and Suction [20] who investigated non-Newtonian dissipative radiative flow, and Bhargava et al. [21] who studied radiative-convection micropolar flow in porous media.

Very few of the above studies have considered *Falkner–Skan flows* [22,23]. This family of boundary layer flows is associated with the two-dimensional wedge configuration. Non-Newtonian flows from wedge bodies arise in a number of chemical engineering systems which have been described in detail by Peddieson [24] employing the second order Reiner–Rivlin model. The mixed convection boundary layer flow from a heated wedge plate has also drawn some interest. The combined forced and free convection flow and heat transfer about a non-isothermal wedge subject to a non-uniform free stream velocity was first considered by Sparrow et al. [25]. Watanabe et al. [26] analyzed theoretically mixed convection flow over a perforated wedge with uniform suction or injection. Kafoussias and Nanousis [27] and Nanousis [28] studied the effect of suction or injection on MHD mixed convection flow past a wedge. Gorla [29] used a power-law model to study heat transfer in polymer flow past a wedge. Yih [30] evaluated radiation effects on mixed convection flow about an isothermal wedge embedded in a saturated porous medium. Rashidi et al. [31] developed homotopy solutions for third grade viscoelastic flow from a non-isothermal wedge. Chamkha et al. [32] presented computational solutions for MHD forced convection flow from a non-isothermal wedge in the presence of a heat source or sink with a finite difference method. Hsiao [33] reported on MHD convection of viscoelastic fluid past a porous wedge, observing that the elastic effect increases the local heat transfer coefficient and heat transfer rates at the wedge surface. Ishak et al. [34] obtained a self-similar solution for a moving wedge in a micropolar fluid. Ishak et al. [35] further studied numerically steady two-dimensional laminar flow past a moving wedge in non-Newtonian fluid. Ishak et al. [36] studied the MHD boundary layer flow of a micropolar fluid past a wedge with constant heat flux. Ishak et al. [37] examined the MHD boundary layer flow of a micropolar fluid past a wedge with variable wall temperature.

The current work presents a numerical study of laminar boundary layer flow, heat and mass transfer of Jeffrey's

non-Newtonian fluid past a non-isothermal wedge with thermal radiation and heat generation/absorption. The non-dimensional equations with associated dimensionless boundary conditions constitute a highly nonlinear, coupled two-point boundary value problem. Keller's implicit finite difference "box" scheme is implemented to solve the problem. The effects of the emerging thermophysical parameters, namely *Deborah number (De), ratio of relaxation to retardation times (λ), pressure gradient parameter (m), radiation parameter (F), Heat source/sink parameter (Δ), and mixed convection parameter (λ_1)*, on the velocity, temperature, concentration, local skin friction, heat transfer rate and mass transfer rate characteristics are studied. The present problem has to the authors' knowledge not appeared thus far in the scientific literature and is relevant to polymeric manufacturing processes and nuclear waste simulations.

2. Mathematical model

The steady, laminar, two-dimensional, incompressible boundary layer flow, heat and mass transfer from a non-isothermal wedge to Jeffrey's fluid in the presence of heat source/sink and thermal radiation is studied, as illustrated in Fig. 1. Both wedge and Jeffrey's fluid are initially maintained at a constant temperature and concentration. Instantaneously, they are raised to a temperature $T_w(> T_\infty)$ and concentration $C_w(> C_\infty)$, where the latter (ambient) temperature and concentration of the fluid are sustained constant. The x-coordinate (tangential) is measured along the wall of the wedge and the y-coordinate (radial) is measured normal to it. The corresponding velocities in x and y directions are u and v respectively. The gravitational acceleration $\boldsymbol{g}$, acts vertically downwards. The Boussinesq approximation holds i.e. the density variation is only experienced in the buoyancy term in the momentum equation. The Cauchy stress tensor, $\boldsymbol{S}$, of a Jeffrey's non-Newtonian fluid [38] takes the form as follows:

$$\boldsymbol{T} = -p\boldsymbol{I} + \boldsymbol{S}, \quad \boldsymbol{S} = \frac{\mu}{1+\lambda}(\dot{\gamma} + \lambda_2 \ddot{\gamma}) \tag{1}$$

where a dot above a quantity denotes the material time derivative and $\dot{\gamma}$ is the shear rate. The Jeffrey's model provides an elegant formulation for simulating retardation and relaxation effects arising in non-Newtonian polymer flows. The shear rate and gradient of shear rate are further defined in terms of velocity vector, $\boldsymbol{V}$, as follows:

$$\dot{\gamma} = \nabla V + (\nabla V)^T \tag{2}$$

$$\ddot{\gamma} = \frac{d}{dt}\left(\dot{\gamma}\right) \tag{3}$$

Introducing the boundary layer approximations, and incorporating the stress tensor for a Jeffrey's fluid in the momentum equation (in differential form), the conservation equations take the form as follows:

$$\frac{\partial u}{\partial x} + \frac{\partial v}{\partial y} = 0 \tag{4}$$

$$u\frac{\partial u}{\partial x} + v\frac{\partial u}{\partial y} = U_\infty \frac{dU_\infty}{dx} + \frac{\nu}{1+\lambda}\left(\frac{\partial^2 u}{\partial y^2} + \lambda_2\left(u\frac{\partial^3 u}{\partial x \partial y^2} - \frac{\partial u}{\partial x}\frac{\partial^2 u}{\partial y^2} + \frac{\partial u}{\partial y}\frac{\partial^2 u}{\partial x \partial y} + v\frac{\partial^3 u}{\partial y^3}\right)\right) + g\beta(T - T_\infty)\sin\left(\frac{\Omega}{2}\right) + g\beta^*(C - C_\infty)\sin\left(\frac{\Omega}{2}\right) \tag{5}$$

$$u\frac{\partial T}{\partial x} + v\frac{\partial T}{\partial y} = \alpha\frac{\partial^2 T}{\partial y^2} - \frac{1}{\rho c_p}\frac{\partial q_r}{\partial y} + \frac{Q_0}{\rho c_p}(T - T_\infty) \tag{6}$$

$$u\frac{\partial C}{\partial x} + v\frac{\partial C}{\partial y} = D_m\frac{\partial^2 C}{\partial y^2} \tag{7}$$

The Jeffrey's fluid model, introduces a number of *mixed* derivatives in the momentum boundary layer Eq. (4) and in particular two *third order* derivatives $u\frac{\partial^3 u}{\partial x \partial y^2}$ and $v\frac{\partial^3 u}{\partial y^3}$, making the system an order higher than the *classical Navier–Stokes (Newtonian) viscous flow* model. The non-Newtonian effects feature in the shear terms only of Eq. (5) and not the convective (acceleration) terms. The third term on the right hand side

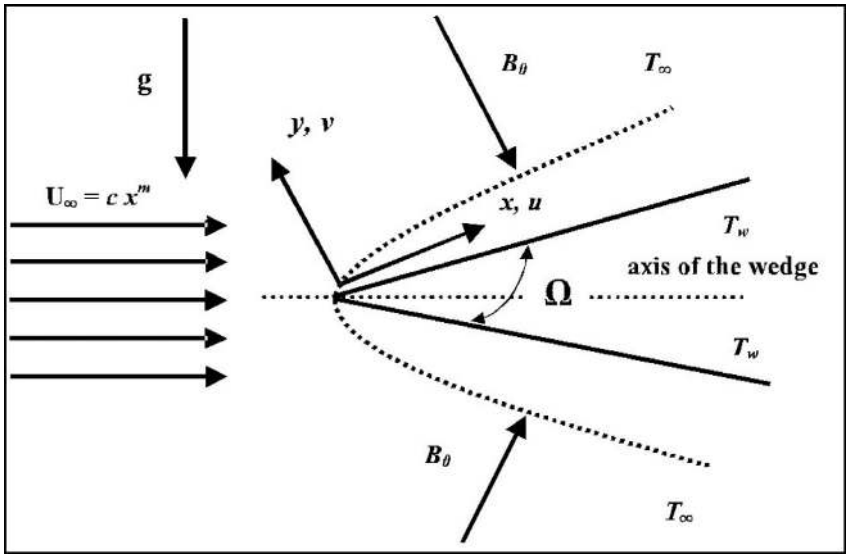

Figure 1 Physical model and coordinate system.

of Eq. (5) represents the *thermal buoyancy force* and couples the velocity field with the temperature field Eq. (6). The fourth term on right hand side of Eq. (5) represents the *species buoyancy effect (mass transfer)* and couples Eq. (5) to the species diffusion Eq. (7). Viscous dissipation effects are neglected in the model.

The appropriate boundary conditions are as follows:

$$\begin{aligned} &At\ \ y=0,\ \ u=0,\ \ v=0,\ \ T=T_w,\ \ C=C_w \\ &As\ \ y\to\infty,\ \ u\to U_\infty=Cx^m,\ \ v\to 0,\ \ T\to T_\infty,\ \ C\to C_\infty \end{aligned} \tag{8}$$

where $U_\infty = Cx^m$ is the free stream velocity, $m = \beta_1/(2-\beta_1)$ is the Hartree pressure gradient parameter which corresponds to $\beta_1 = \Omega/\pi$ for a total angle Ω of the wedge, and C is a positive number.

In Eq. (6) the penultimate term on the right side is the thermal radiation flux contribution based on Rosseland approximation [39,40]. This formulation allows the transformation of the governing integro-differential equation for radiative energy balance into electrostatic potential (Coulomb's law) which is valid for optically-thick media in which radiation only propagates a limited distance prior to experiencing scattering or absorption. It can be shown that the local intensity is caused by radiation emanating from nearby locations in the vicinity of which the emission and scattering are comparable to the location under consideration. For zones where conditions are appreciably different, the radiation has been shown to be greatly attenuated prior to arriving at the location being analyzed. The energy transfer depends only on the conditions in the area near the position under consideration. In applying the Rosseland assumption, it is assumed that refractive index of the medium is constant, intensity within the porous medium is nearly isotropic and uniform and wavelength regions exist where the optical thickness is greater than 5. Further details are available in Bég et al. [41]. The final term on the right hand side of Eq. (6) is the *heat source/sink contribution*. The Rosseland diffusion flux model is an *algebraic approximation* and defined as follows:

$$q_r = \frac{4\sigma^*}{3k^*}\frac{\partial T^4}{\partial y} \tag{9}$$

where k^* – mean absorption coefficient and σ^* – Stefan–Boltzmann constant. It is customary [42] to express T^4 as a linear function of temperature. Expanding T^4 using Taylor series and neglecting higher order terms lead to

$$T^4 \cong 4T_\infty^3 T - 3T_\infty^4 \tag{10}$$

Substituting (10) into (9), eventually leads to the following version of the heat conservation Eq. (6):

$$u\frac{\partial T}{\partial x} + v\frac{\partial T}{\partial y} = \alpha\frac{\partial^2 T}{\partial y^2} + \frac{16\sigma^* T_\infty^3}{3k^*\rho c_p}\frac{\partial^2 T}{\partial y^2} + \frac{Q_0}{\rho c_p}(T-T_\infty) \tag{11}$$

To transform the boundary value problem to a dimensionless one, we introduce a stream function Ψ defined by the *Cauchy–Riemann* equations, $u = \frac{\partial \Psi}{\partial y}$ and $v = -\frac{\partial \Psi}{\partial x}$.

The mass conservation Eq. (4) is automatically satisfied.

The following dimensionless variables are introduced into Eqs. (5)–(8):

$$\begin{aligned} &\xi = \frac{\sigma x}{\rho U_\infty},\quad \eta = \frac{y}{x}Re_x^{1/2},\quad f = \frac{\psi}{(U_\infty x\nu)^{1/2}}, \\ &\theta(\xi,\eta) = \frac{T-T_\infty}{T_w-T_\infty},\quad \phi(\xi,\eta) = \frac{C-C_\infty}{C_w-C_\infty} \\ &Pr = \frac{\nu\rho c_p}{k},\quad Sc = \frac{\nu}{D_m},\quad Gr_x = \frac{g\beta(T_w-T_\infty)x^3}{4\nu^2}, \\ &De = \frac{\lambda_2 \nu Re_x}{x^2},\quad Re_x = \frac{U_\infty x}{\nu},\quad \lambda_1 = \frac{Gr_x}{Re_x} \end{aligned} \tag{12}$$

The resulting momentum, energy and concentration boundary layer equations take the form as follows:

$$\begin{aligned} &\frac{f'''}{1+\lambda} + \frac{1+m}{2}ff'' - m(f')^2 + m + \lambda_1(\theta+N\phi)\sin\left(\frac{\Omega}{2}\right) \\ &-\frac{De}{1+\lambda}\left(\begin{matrix}(1-m)f'f''' - \frac{3m-1}{2}f''^2 \\ +\frac{1+m}{2}ff^{iv}\end{matrix}\right) \\ &= \xi(1-m)\left(f'\frac{\partial f'}{\partial \xi} - f''\frac{\partial f}{\partial \xi} - \frac{De}{1+\lambda}\left(f'\frac{\partial f'''}{\partial \xi} - f'''\frac{\partial f'}{\partial \xi} + f''\frac{\partial f''}{\partial \xi} - f^{iv}\frac{\partial f}{\partial \xi}\right)\right) \end{aligned} \tag{13}$$

$$\frac{\theta''}{Pr}\left(1+\frac{4}{3F}\right) + \frac{1+m}{2}f\theta' + \Delta\theta = \xi(1-m)\left(f'\frac{\partial \theta}{\partial \xi} - \theta'\frac{\partial f}{\partial \xi}\right) \tag{14}$$

$$\frac{\phi''}{Sc} + \frac{1+m}{2}f\phi' = \xi(1-m)\left(f'\frac{\partial \phi}{\partial \xi} - \phi'\frac{\partial f}{\partial \xi}\right) \tag{15}$$

The corresponding non-dimensional boundary conditions for the collectively eighth order, multi-degree partial differential equation system defined by Eqs. (13)–(15) assume the following form:

$$\begin{aligned} &At\quad \eta=0,\quad f=0,\quad f'=0,\quad \theta=1,\quad \phi=1 \\ &As\quad \eta\to\infty,\quad f'\to 1,\quad f''\to 0,\quad \theta\to 0,\quad \phi\to 0 \end{aligned} \tag{16}$$

Here primes denote the differentiation with respect to η. $N = \frac{\beta^*(C_w-C_\infty)}{\beta(T_w-T_\infty)}$ – concentration to thermal buoyancy ratio parameter, $F = \frac{Kk^*}{4\sigma^* T_\infty^3}$ – the radiation parameter, $\Delta = \frac{Q_0 x^2}{\rho c_p Re_x}$ – the dimensionless heat generation/absorption coefficient.

The skin-friction coefficient (shear stress at the wedge surface), Nusselt number (heat transfer rate) and Sherwood number (mass transfer rate) can be defined using the transformations described above with the following expressions:

$$\frac{C_f}{Re_x^{1/2}} = f''(\xi,0) \tag{17}$$

$$\frac{Nu_x}{Re_x^{1/2}} = -\theta'(\xi,0) \tag{18}$$

$$\frac{Sh_x}{Re_x^{1/2}} = -\phi'(\xi,0) \tag{19}$$

The location, $\xi \sim 0$, corresponds to the vicinity of the *lower stagnation point* on the wedge. For this scenario, the model defined by Eqs. (13)–(15) contracts to an *ordinary* differential boundary value problem:

$$\begin{aligned} &\frac{f'''}{1+\lambda} + \frac{1+m}{2}ff'' - m(f')^2 + m + \lambda_1(\theta+N\phi)\sin\left(\frac{\Omega}{2}\right) \\ &-\frac{De}{1+\lambda}\left(\begin{matrix}(1-m)f'f''' - \frac{3m-1}{2}f''^2 \\ +\frac{1+m}{2}ff^{iv}\end{matrix}\right) = 0 \end{aligned} \tag{20}$$

$$\frac{\theta''}{Pr}\left(1+\frac{4}{3F}\right)+\frac{1+m}{2}f\theta'+\Delta\theta=0 \tag{21}$$

$$\frac{\phi''}{Sc}+\frac{1+m}{2}f\phi'=0 \tag{22}$$

3. Computational finite difference solutions

The Keller-Box implicit difference method is utilized to solve the nonlinear boundary value problem defined by Eqs. (13)–(15) with boundary conditions (16). This technique, despite recent developments in other numerical methods, remains a powerful and very accurate approach for boundary layer flow equation systems *which are generally parabolic in nature*. It is unconditionally stable and achieves exceptional accuracy. An excellent summary of this technique is given in Keller [42]. Magnetohydrodynamics applications of Keller's method are reviewed in Bég [43]. This method has also been applied successfully in many rheological flow problems in recent years. These include oblique micropolar stagnation flows [44], Walter's B viscoelastic flows [45], Stokesian couple stress fluids [46], hyperbolic-tangent convection flows from curved bodies [47], micropolar nanofluids [48], Jeffrey's elasto-viscous boundary layers [14], magnetic Williamson fluids [49] and Maxwell fluids [50]. The Keller-Box discretization is *fully coupled* at each step which reflects the physics of parabolic systems – which are also fully coupled. Discrete calculus associated with the Keller-Box scheme has also been shown to be fundamentally different from all other mimetic (physics capturing) numerical methods, as elaborated by Keller [42]. The Keller Box Scheme comprises four stages:

(1) Reduction of the Nth order partial differential equation system to N first order equations.
(2) Finite Difference Discretization.
(3) Quasilinearization of Non-Linear Keller Algebraic Equations.
(4) Block-tridiagonal Elimination of Linear Keller Algebraic Equations.

4. Results and discussion

Comprehensive results are obtained and are presented in Tables 1–4 and Figs. 2–10. The numerical problem comprises of two independent variables (ξ, η), three dependent fluid dynamic variables (f, θ, ϕ) and nine thermo-physical and body force control parameters, namely, De, λ, Δ, λ_1, F, m, N, Pr, Sc. The following default parameter values i.e. $De = 0.1$, $\lambda = 0.2$, $\Delta = 0.1$, $\lambda_1 = 0.1$, $F = 0.5$, $m = 0.2$, $N = 0.5$, $Pr = 0.71$, $Sc = 0.6$ are prescribed (unless otherwise stated).

Table 1 depicts the influence of increasing Sc, De on skin friction, heat transfer rate and mass transfer rate, along with a variation in λ and transverse coordinate (ξ). Increasing Sc, which implies a decrease in mass diffusivity of the species is observed to suppress skin friction and heat transfer rate whereas it enhances the mass transfer rate. With an increase in λ, skin friction is strongly boosted as are heat transfer rate and mass transfer rate. Also, increasing De reduces skin friction, heat transfer rate and mass transfer rate.

Table 2 presents the influence of increasing parameter λ_1, N on skin friction, heat transfer rate and mass transfer rates, along with a variation in Pr and transverse coordinate, ξ. With increasing λ_1, it is observed that the skin friction, heat transfer rate and mass transfer rate increase significantly. An increase in N is found to enhance skin friction, heat transfer rate and mass transfer rate. And an increase in Pr is observed to reduce skin friction and mass transfer rate but increases heat transfer rate.

Table 3 presents the influence of increasing Δ and m on skin friction, heat transfer rate and mass transfer rate, along with a variation in F and the transverse coordinate, ξ. Increasing m, is found to increase skin friction, heat transfer rate and mass transfer rate. This trend is sustained for all values of transverse coordinate. An increase in Δ boosts skin friction but heat transfer rate is reduced markedly but mass transfer rate is increased slightly. Increasing F is observed to decrease skin friction and mass transfer rate whereas the heat transfer rate is increased markedly.

Table 4 presents the values of skin friction and heat transfer for different values of λ and the values are compared with those of Minkowycz et al. [51]. The present work values are found to be in good correlation with [51].

In Fig. 2(a)–(c), the evolution of velocity (f'), temperature (θ) and concentration (ϕ) functions with a variation in De, is depicted. Dimensionless velocity (Fig. 2(a)) is considerably decreased with increasing De. De clearly arises in connection with high order derivatives in Eq. (13) i.e. $\frac{De}{1+\lambda}[(1-m)f'f''-\frac{3m-1}{2}f''^2+\frac{1+m}{2}ff^{iv}]$ and $\xi\left(-\frac{De}{1+\lambda}\left[f'\frac{\partial f'''}{\partial\xi}-f'''\frac{\partial f'}{\partial\xi}+f''\frac{\partial f''}{\partial\xi}-f^{iv}\frac{\partial f}{\partial\xi}\right]\right)$. In Fig. 2(b), an increase in De is seen to considerably increase temperatures throughout the boundary layer regime. Although De does not arise in the thermal boundary layer Eq. (14), there is a strong coupling of this equation with the momentum field via the convective terms $\xi\left[f'\frac{\partial\theta}{\partial\xi}\right]$ and $\xi\left[-\theta'\frac{\partial f}{\partial\xi}\right]$. Furthermore, the thermal buoyancy force term, $+\theta$ in the momentum Eq. (13) strongly couples the momentum flow field to the temperature field. Thermal boundary layer thickness is also elevated with increasing De. Fig. 2(c) shows a slight increase in concentration is achieved with increasing De values.

Fig. 3(a)–(c) illustrates the effect of λ on the velocity (f'), temperature (θ) and concentration (ϕ) distributions through the boundary layer regime. Velocity is significantly increased with increasing λ. The polymer flow is therefore considerably a*ccelerated* with an increase in relaxation time (or decrease in retardation time). The temperature is also increased with increasing λ. Conversely, temperature and concentration are depressed markedly with increasing λ. The mathematical model reduces to the *Newtonian viscous flow model* as $\lambda \to 0$ and $De \to 0$, since this negates relaxation, retardation and elasticity effects. The momentum boundary layer equation in these cases contracts to the familiar equation for *Newtonian mixed convection* from a wedge:

$$f'''+\frac{1+m}{2}ff''-mf'^2+m+\lambda(\theta+N\phi)\sin\left(\frac{\Omega}{2}\right)=\xi(1-m)\left(f'\frac{\partial f'}{\partial\xi}-f''\frac{\partial f}{\partial\xi}\right) \tag{23}$$

Table 1 Values of C_f, Nu and Sh for various values of De, λ and Sc ($Pr = 0.71$, $N = 0.5$, $\Delta = 0.1$, $F = 0.5$, $\lambda_1 = 0.1$, $\Omega = 30^0$, $m = 0.2$).

De	λ	Sc	$\xi = 1.0$			$\xi = 2.0$			$\xi = 3.0$		
			C_f	Nu	Sh	C_f	Nu	Sh	C_f	Nu	Sh
0.05	0.2	0.6	0.5578	0.2164	0.3267	0.5523	0.2155	0.3256	0.4601	0.1523	0.3027
0.1			0.5510	0.2147	0.3234	0.5479	0.2142	0.3229	0.4601	0.1523	0.3027
0.35			0.5348	0.2136	0.3211	0.5313	0.2134	0.3209	0.4601	0.1523	0.3027
0.65			0.5287	0.2127	0.3190	0.5204	0.2126	0.3190	0.4601	0.1523	0.3027
1.0			0.5159	0.2108	0.3070	0.5120	0.2105	0.3060	0.4601	0.1523	0.3027
0.1	0.0	0.6	0.5141	0.2140	0.3210	0.5102	0.2131	0.3198	0.4601	0.1523	0.3027
	0.5		0.3202	0.2186	0.3324	0.6154	0.2178	0.3316	0.4601	0.1523	0.3027
	1.0		0.7108	0.2218	0.3406	0.7051	0.2211	0.3400	0.4601	0.1523	0.3027
	1.5		0.7911	0.2242	0.3468	0.7847	0.2237	0.3465	0.4601	0.1523	0.3027
	2.0		0.8642	0.2261	0.3518	0.8567	0.2257	0.3515	0.4601	0.1523	0.3027
0.1	0.2	0.25	0.5606	0.2162	0.2580	0.5563	0.2153	0.2571	0.4601	0.1523	0.3027
		0.78	0.5582	0.2160	0.3559	0.5539	0.2151	0.3548	0.4601	0.1523	0.3027
		0.94	0.5577	0.2160	0.3799	0.5534	0.2151	0.3787	0.4601	0.1523	0.3027
		1.25	0.5569	0.2159	0.4209	0.5526	0.2151	0.4193	0.4601	0.1523	0.3027
		1.75	0.5560	0.2158	0.4751	0.5516	0.2150	0.4734	0.4601	0.1523	0.3027
		2.0	0.5556	0.2158	0.4985	0.5512	0.2150	0.4968	0.4601	0.1523	0.3027

Table 2 Values of C_f, Nu and Sh for various values of λ_1, N and Pr ($De = 0.1$, $Sc = 0.6$, $\Delta = 0.1$, $F = 0.5$, $\lambda = 0.2$, $\Omega = 30^0$, $m = 0.2$).

λ_1	N	Pr	$\xi = 1.0$			$\xi = 2.0$			$\xi = 3.0$		
			C_f	Nu	Sh	C_f	Nu	Sh	C_f	Nu	Sh
−0.2	0.5	0.71	0.3981	0.2035	0.3096	0.3925	0.2085	0.3074	0.3906	0.2080	0.3065
−0.1			0.4533	0.2067	0.3153	0.4483	0.2108	0.3136	0.4465	0.2104	0.3189
0.0			0.5069	0.2096	0.308	0.5022	0.2130	0.3194	0.5006	0.2127	0.3189
0.1			0.5589	0.2122	0.3261	0.5546	0.2152	0.3250	0.530	0.2149	0.3246
0.3			0.6591	0.2170	0.3361	0.6552	0.2192	0.3354	0.6537	0.2190	0.3351
0.2	−0.5	0.71	0.5276	0.2108	0.3231	0.5231	0.2140	0.3219	0.5215	0.2137	0.3214
	0.0		0.5433	0.2115	0.3246	0.5389	0.2146	0.3235	0.5373	0.2143	0.3230
	1.0		0.5744	0.2129	0.3276	0.5701	0.2158	0.3265	0.5685	0.2155	0.3261
	2.0		0.6049	0.2143	0.3304	0.6007	0.2169	0.3295	0.5992	0.2167	0.3291
0.2	0.5	0.5	0.5594	0.2080	0.3262	0.5551	0.2106	0.3251	0.5535	0.2103	0.3247
		1.0	0.5583	0.2184	0.3260	0.5540	0.2217	0.3249	0.5524	0.2214	0.3245
		2.0	0.5563	0.2397	0.3256	0.5519	0.2445	0.3245	0.5503	0.2441	0.3241
		3.0	0.5545	0.2594	0.3253	0.5501	0.2652	0.3242	0.548	0.2649	0.3237
		5.0	0.5519	0.2901	0.3248	0.5475	0.2975	0.3237	0.5459	0.2972	0.3233
		7.0	0.5502	0.3108	0.3245	0.5458	0.3193	0.3234	0.5441	0.3190	0.3230

The thermal boundary layer equation and concentration Eqs. (14) and (15) remain unchanged.

Fig. 4(a)–(c) presents typical profiles for velocity (f'), temperature (θ) and concentration (ϕ) for various values of F. Increasing F, strongly decelerates the flow i.e. decreases velocity. This parameter features in the term, $\frac{1}{Pr}\left(1+\frac{4}{3F}\right)\theta''$ in the energy conservation Eq. (14). F represents the relative contribution of *thermal conduction* to *thermal radiation* heat transfer. For $F = 1$ both models of heat transfer have the same contribution. Temperatures are therefore also decreased, as observed in Fig. 4(b). Conversely, there is a slight enhancement in concentration values with increasing F values, as shown in Fig. 4(c).

Fig. 5(a)–(c) depicts the velocity (f'), temperature (θ) and concentration (ϕ) distributions with the variation in λ_1. Clearly, from these figures it can be seen that as λ_1 increases, the fluid velocity increases. Fig. 5(b) shows the effect of λ_1 on the temperature profiles. It is noticed that temperature profiles decrease with an increase in λ_1. A strong decrease in concentration is observed as shown in Fig. 5(c) with the increasing λ_1.

Fig. 6(a)–(c) presents typical profiles for velocity (f'), temperature (θ) and concentration (ϕ) for various values of Δ. Increasing heat generation ($\Delta > 0$) significantly accelerates the flow and also increases temperature magnitudes but reduces concentration values. Conversely, with a heat sink

Table 3 Values of C_f, Nu and Sh for various values of Δ, F and m ($De = 0.1$, $\lambda = 0.2$, $Pr = 0.71$, $N = 0.5$, $Sc = 0.6$, $F = 0.5$, $\lambda_1 = 0.1$).

Δ	m	F	$\xi = 1.0$			$\xi = 2.0$			$\xi = 3.0$		
			C_f	Nu	Sh	C_f	Nu	Sh	C_f	Nu	Sh
−2.0	0.2	0.5	0.6000	0.6691	0.3993	0.5958	0.6674	0.3977	0.5947	0.6667	0.3971
−1.0			0.6019	0.5192	0.3994	0.5976	0.5251	0.3978	0.5960	0.5245	0.3972
0.0			0.6043	0.3512	0.3996	0.6001	0.3555	0.3980	0.5985	0.3551	0.3974
0.2			0.6049	0.3132	0.3996	0.6006	0.3171	0.3981	0.5991	0.3167	0.3975
0.5			0.6059	0.2527	0.997	0.6016	0.2561	0.3981	0.6000	0.2558	0.3976
0.1	−0.02	0.5	0.4084	0.2046	0.2990	0.4096	0.2041	0.2988	0.4099	0.2088	0.2041
	0.1		0.4914	0.2083	0.3126	0.4890	0.2100	0.3124	0.4885	0.2098	0.3123
	0.2		0.5589	0.2122	0.3261	0.5546	0.2152	0.3250	0.5530	0.2149	0.3246
	0.3		0.6259	0.2162	0.3398	0.6191	0.2205	0.3377	0.6197	0.2200	0.3369
	0.4		0.6917	0.2202	0.3531	0.6824	0.2216	0.3502	0.6791	0.2253	0.3492
0.1	0.2	0.1	0.5601	0.2020	0.3263	0.5558	0.2040	0.3253	0.5542	0.2038	0.3248
		1.0	0.5580	0.2253	0.3259	0.5537	0.2244	0.3249	0.5521	0.2240	0.3244
		1.5	0.5575	0.2312	0.3258	0.5531	0.2304	0.3247	0.5515	0.2301	0.3243
		2.0	0.5571	0.2354	0.3258	0.5528	0.2346	0.3247	0.5512	0.2343	0.3242

Table 4 Comparison values of $f''(\xi,0)$ and $-\theta'(\xi,0)$ for various values of λ.

λ	Minkowycz et al. [51]		Present	
	$f''(\xi,0)$	$-\theta'(\xi,0)$	$f''(\xi,0)$	$-\theta'(\xi,0)$
0	0.33206	0.29268	0.33205	0.29268
0.2	0.55713	0.33213	0.55712	0.33212
0.4	0.75041	0.35879	0.75038	0.35878
0.6	0.92525	0.37937	0.92522	0.37936
0.8	1.08792	0.39640	1.08789	0.39638
1.0	1.24170	0.41106	1.24169	0.41104
2.0	1.92815	0.46524	1.92814	0.46523
10.0	5.93727	0.64956	5.93725	0.64955

present, ($\Delta < 0$) the flow is retarded (momentum boundary layer thickness is lowered), and thermal boundary layer thickness is reduced whereas, concentration boundary layer thickness increases.

Fig. 7(a)–(c) depicts the profiles for velocity (f'), temperature (θ) and concentration (ϕ) for various values of m. It is observed that an increase in m significantly accelerates the flow i.e., velocity increases as shown in Fig. 7(a), whereas, increasing m is found to decrease temperature and concentration as shown in Fig. 7(b) and (c).

Fig. 8(a)–(c) depicts the profiles for velocity (f'), temperature (θ) and concentration (ϕ) for various values of N. Increasing N is found to accelerate the flow i.e., velocity increases. However, increasing N is found to reduce both temperature and concentration.

Fig. 9(a)–(c) presents the influence of Deborah number, De on dimensionless skin friction coefficient ($f''(\xi,0)$), heat transfer rate ($-\theta'(\xi,0)$) and mass transfer rate ($-\phi'(\xi,0)$) at the wedge surface. It is observed that the dimensionless skin friction is decreased with an increase in De i.e. the boundary layer flow is decelerated with *greater elasticity effects* in the non-Newtonian fluid. Likewise, on the other hand the heat transfer rate is also substantially decreased with increasing De values. There is also a progressive decay in heat transfer rate (local Nusselt number) with increasing tangential coordinate i.e. ξ-value. A decrease in heat transfer rate at the wall will imply less heat is convected from the fluid regime to the wedge, thereby heating the boundary layer. The mass transfer rate (local Sherwood number) is also found to be suppressed with increasing values of De and furthermore, plummets with further distance from the lower stagnation point (i.e. higher ξ values).

Fig. 10(a)–(c) illustrates the response to the parameter ratio of relaxation and retardation times, λ, on the dimensionless skin friction coefficient ($\xi f''(\xi,0)$), heat transfer rate ($-\theta'(\xi,0)$) and mass transfer rate ($-\phi'(\xi,0)$) at the wedge surface. The skin friction at the wedge surface is accentuated with increasing λ. Also there is a strong elevation in shear stress (skin friction coefficient) with increasing value of the tangential coordinate, ξ. The flow is therefore strongly accelerated along the curved wedge surface away from the lower stagnation point. Heat (local Nusselt number) and mass transfer (local Sherwood number) rates are increased with increasing, λ, *although not as profoundly as the skin friction*. With increasing values of the tangential coordinate, ξ, however both local Nusselt number and local Sherwood number are depressed. As elaborated earlier these characteristics are only maximized at the lower stagnation point.

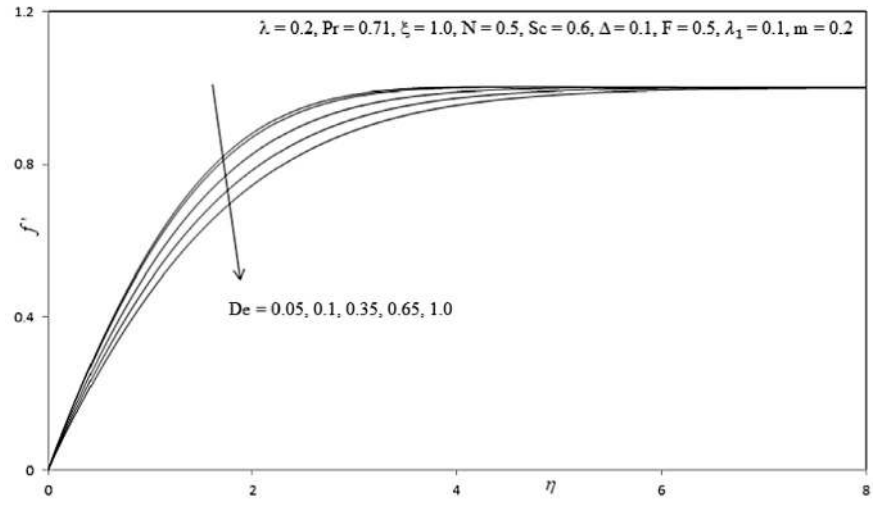

(a) Influence of De on Velocity Profiles

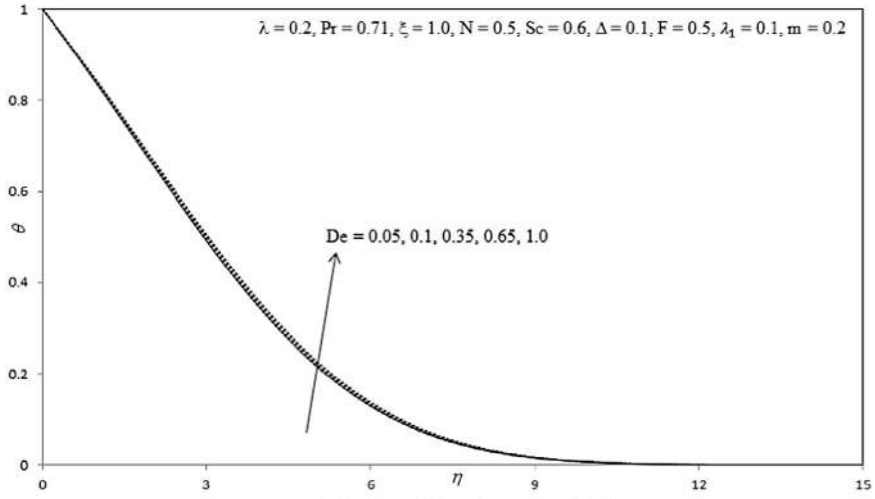

(b) Influence of De on Temperature Profiles

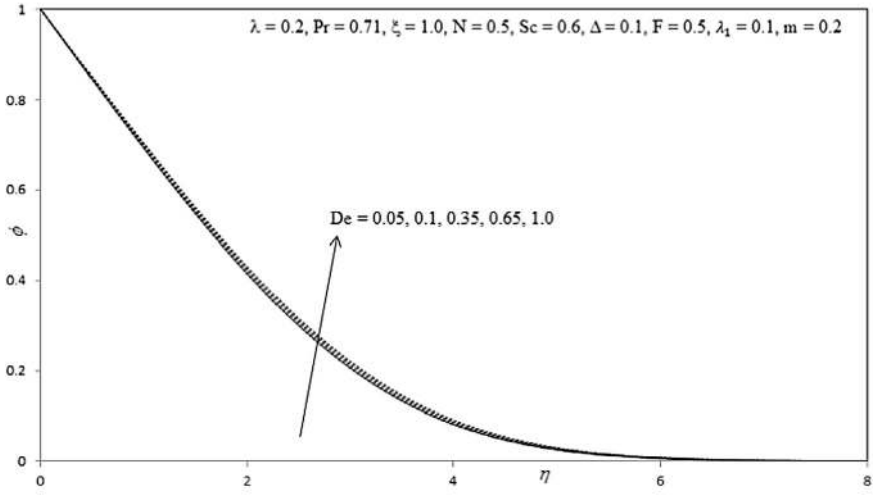

(c) Influnce of De on Concentration Profiles

Figure 2 (a) Influence of *De* on velocity profiles. (b) Influence of *De* on temperature profiles. (c) Influence of *De* on concentration profiles.

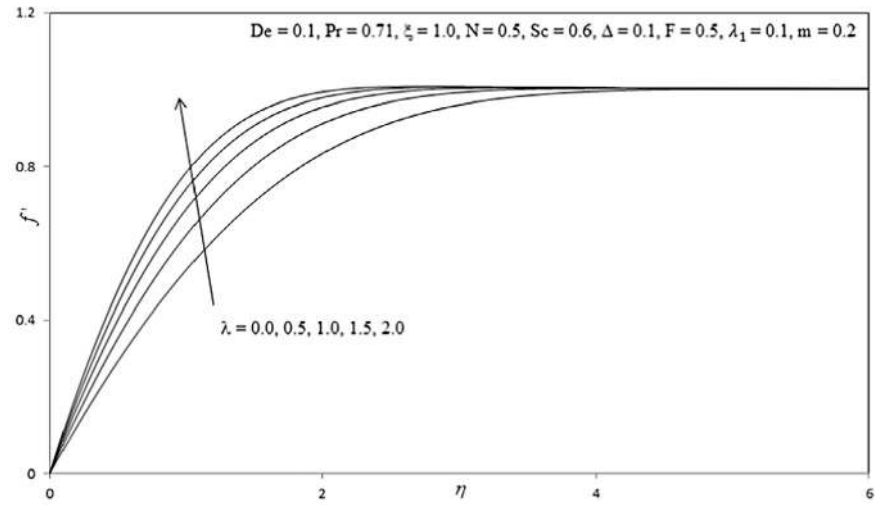

(a) Influence of λ on Velocity Profiles

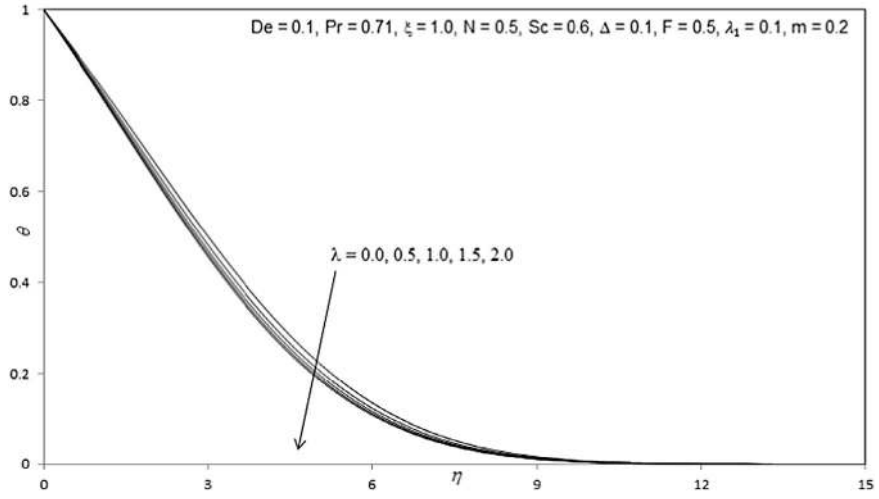

(b) Influence of λ on Temperature Profiles

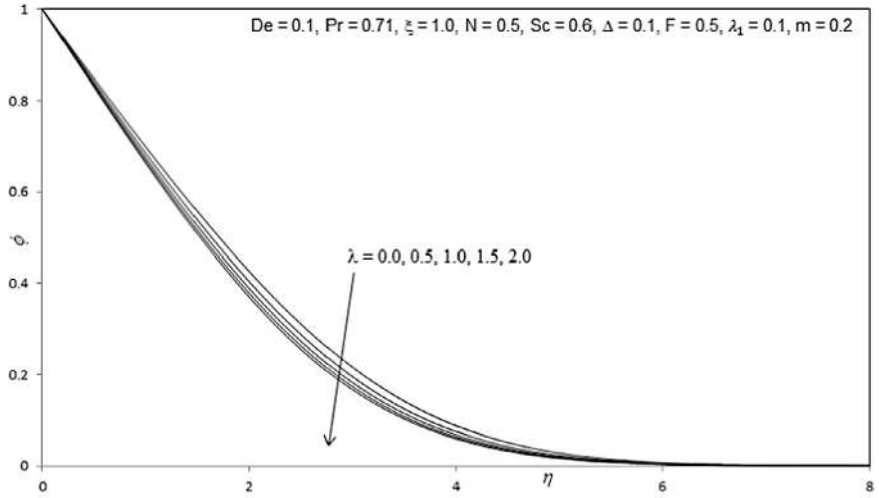

(c) Influnce of λ on Concentration Profiles

Figure 3 (a) Influence of λ on velocity profiles. (b) Influence of λ on temperature profiles. (c) Influence of λ on concentration profiles.

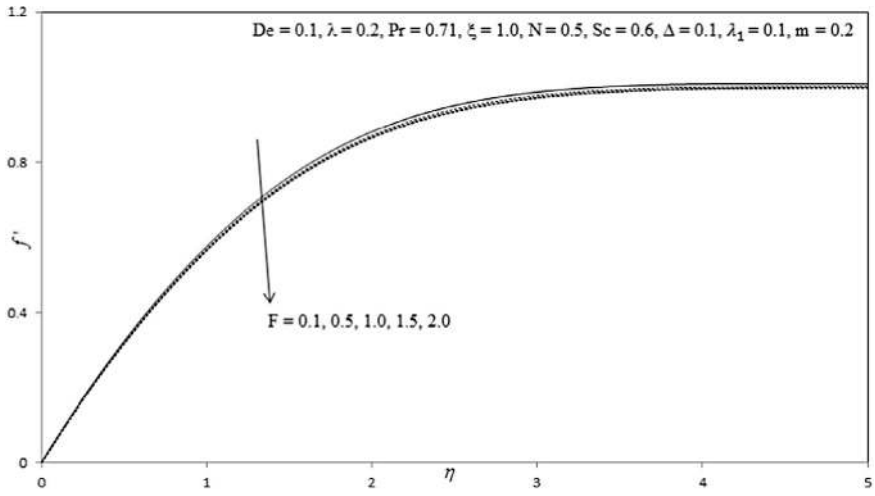

(a) Influence of F on Velocity Profiles

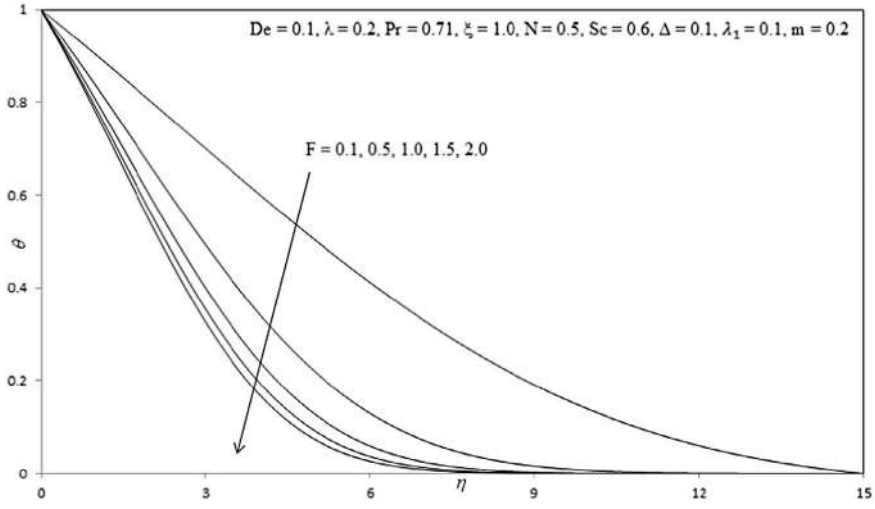

(b) Influence of F on Temperature Profiles

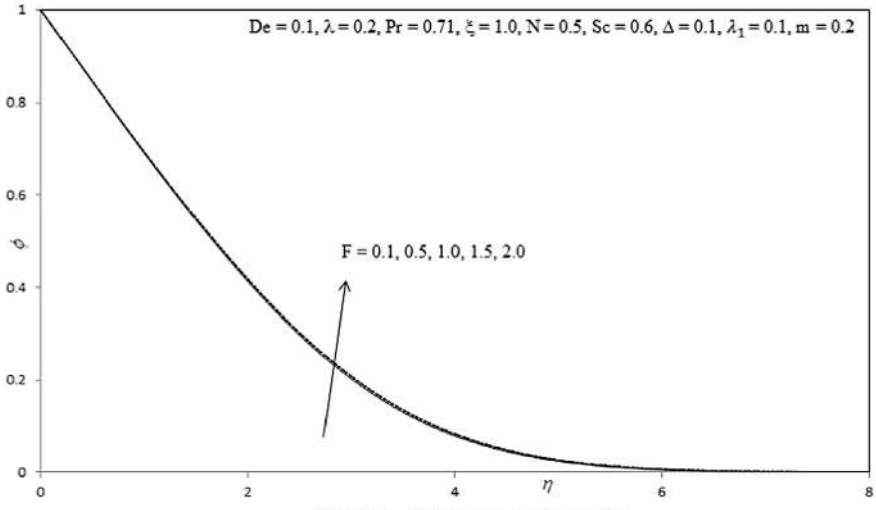

(c) Influnce of F on Concentration Profiles

Figure 4 (a) Influence of F on velocity profiles. (b) Influence of F on temperature profiles. (c) Influence of F on concentration profiles.

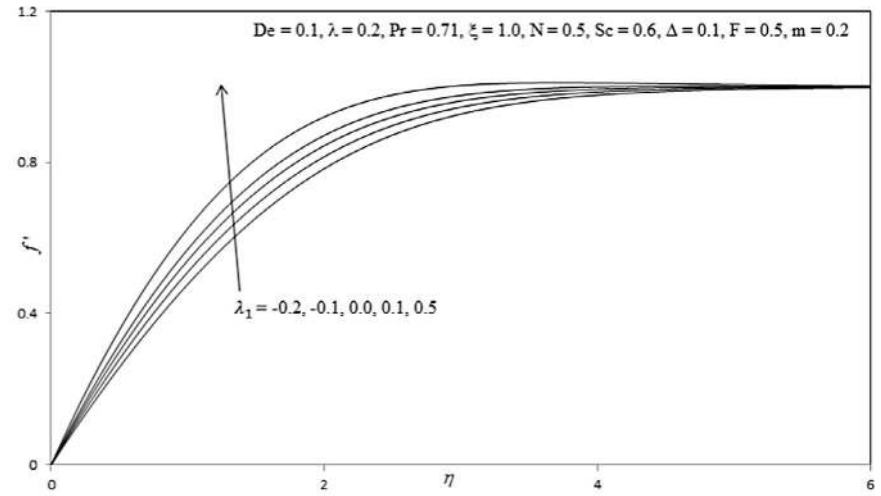

(a) Influence of λ_1 on Velocity Profiles

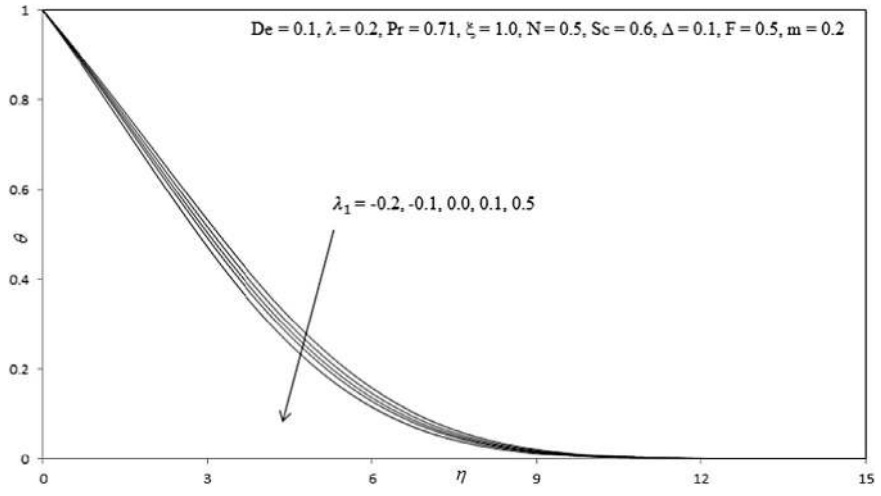

(b) Influence of λ_1 on Temperature Profiles

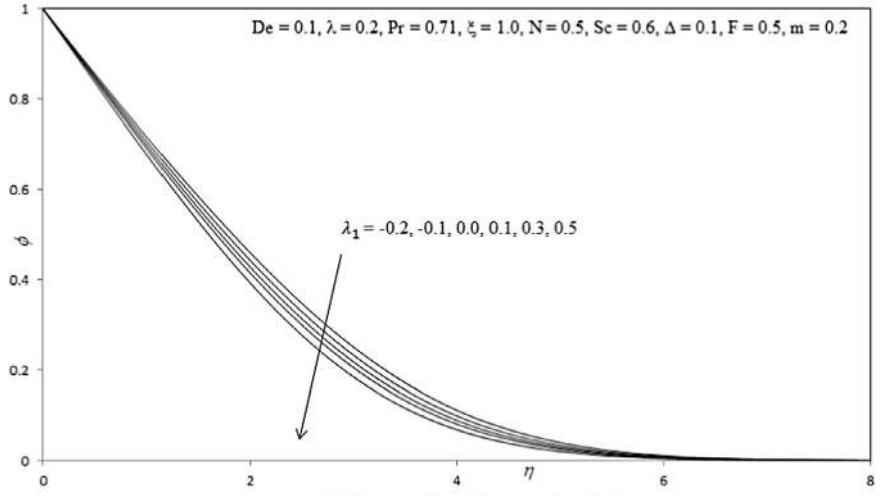

(c) Influnce of λ_1 on Concentration Profiles

Figure 5 (a) Influence of λ_1 on velocity profiles. (b) Influence of λ_1 on temperature profiles. (c) Influence of λ_1 on concentration profiles.

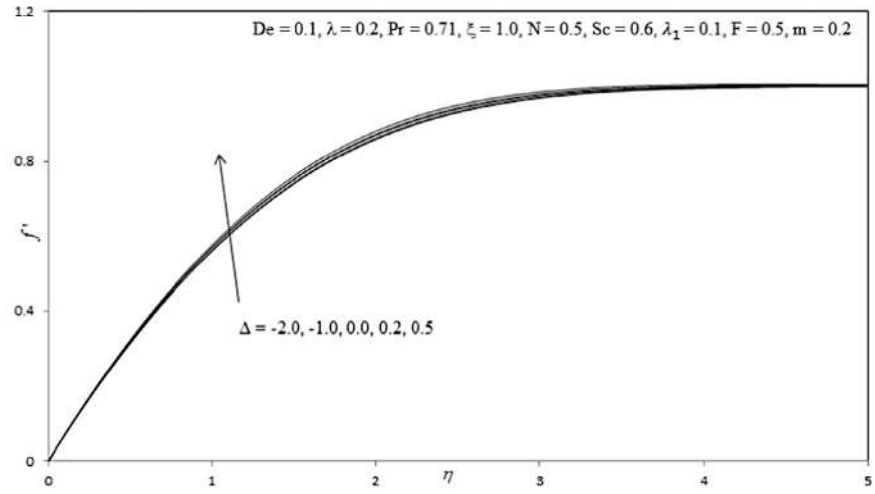

(a) Influence of Δ on Velocity Profiles

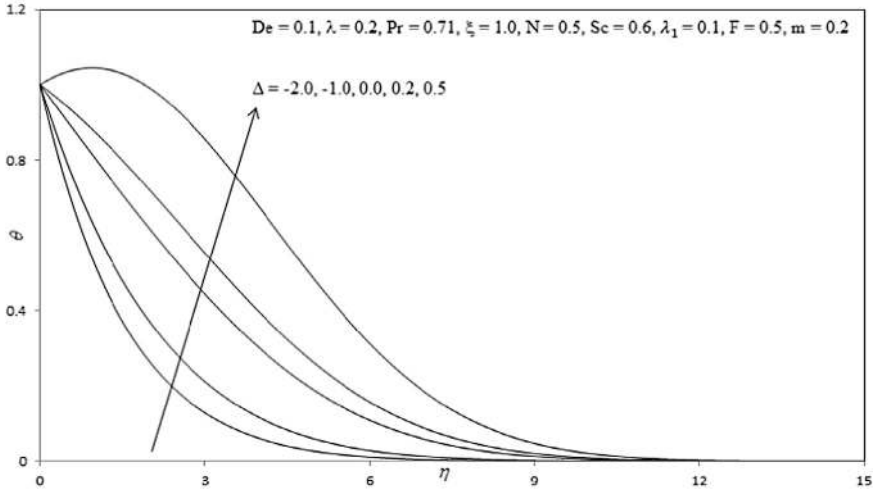

(b) Influence of Δ on Temperature Profiles

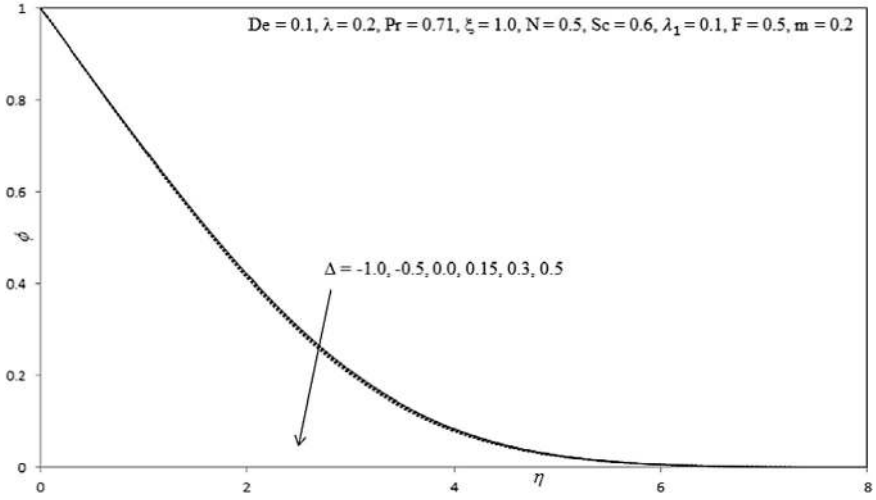

(c) Influnce of Δ on Concentration Profiles

Figure 6 (a) Influence of Δ on velocity profiles. (b) Influence of Δ on temperature profiles. (c) Influence of Δ on concentration profiles.

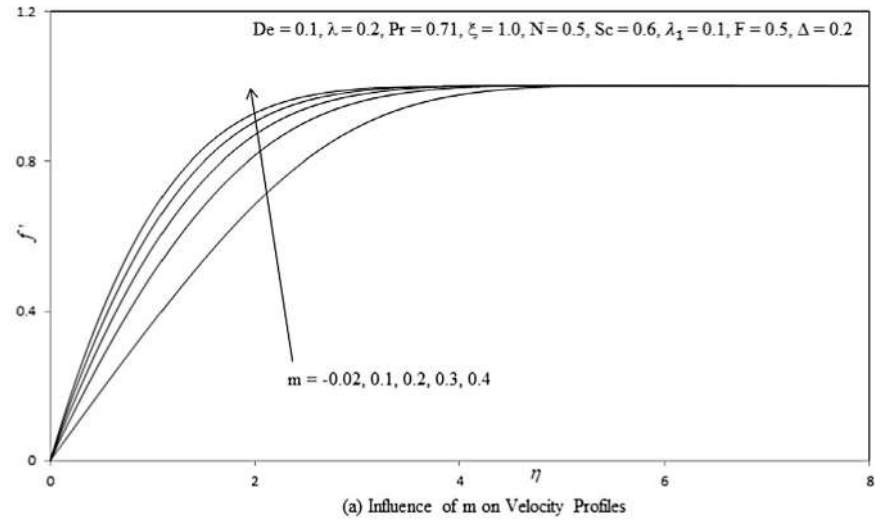

(a) Influence of m on Velocity Profiles

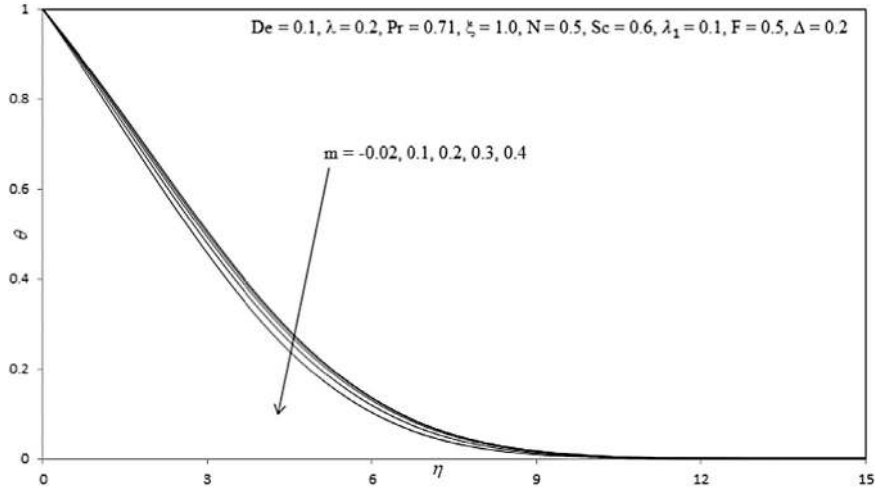

(b) Influence of m on Temperature Profiles

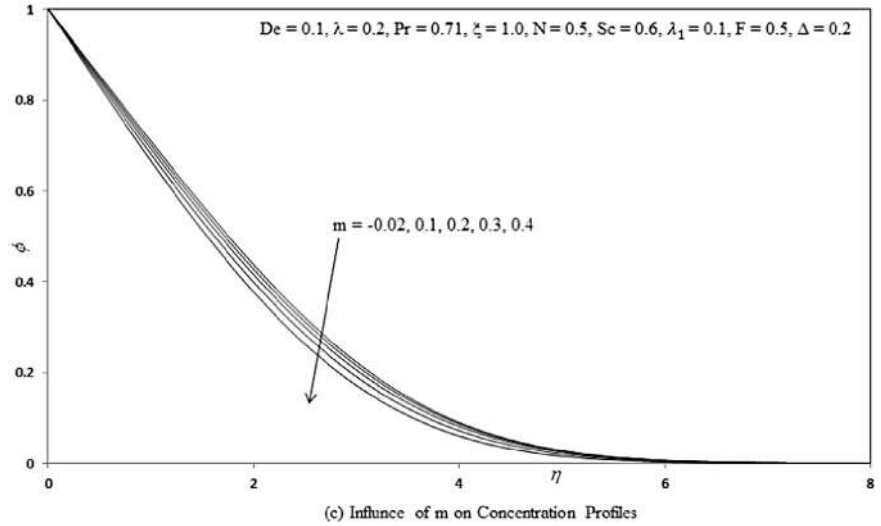

(c) Influnce of m on Concentration Profiles

Figure 7 (a) Influence of m on velocity profiles. (b) Influence of m on temperature profiles. (c) Influence of m on concentration profiles.

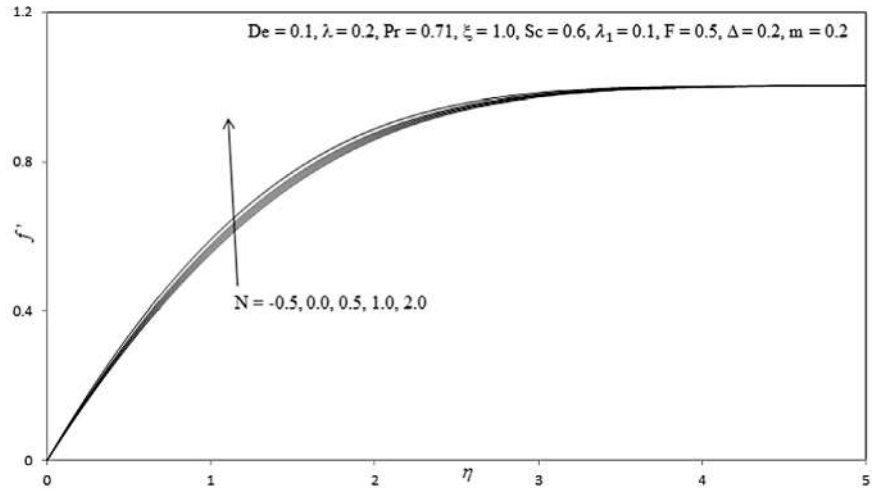

(a) Influence of N on Velocity Profiles

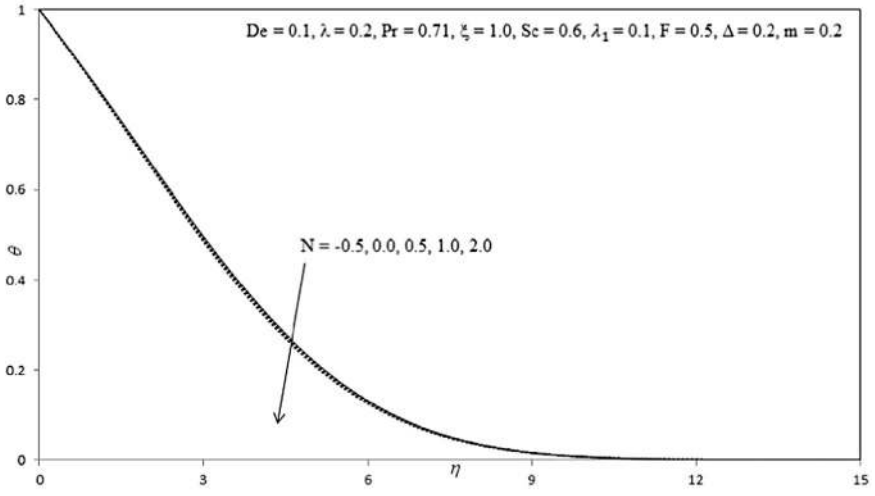

(b) Influence of N on Temperature Profiles

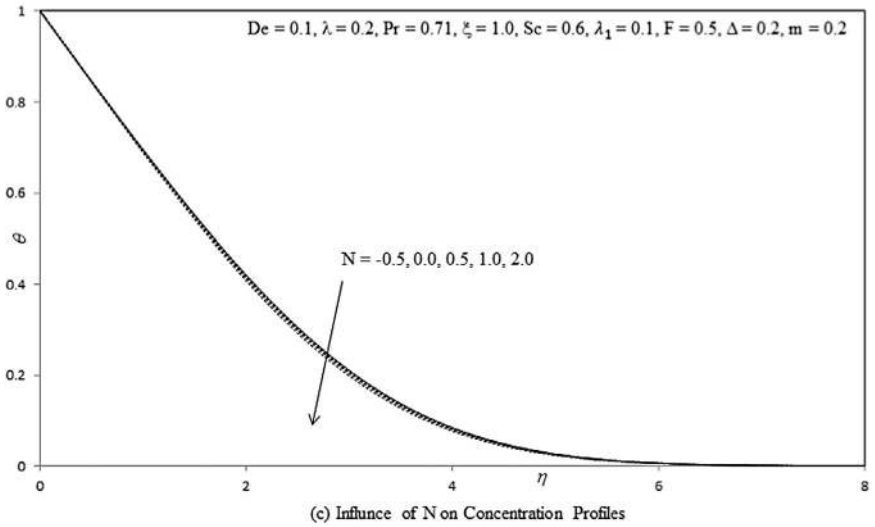

(c) Influnce of N on Concentration Profiles

Figure 8 (a) Influence of N on velocity profiles. (b) Influence of N on temperature profiles. (c) Influence of N on concentration profiles.

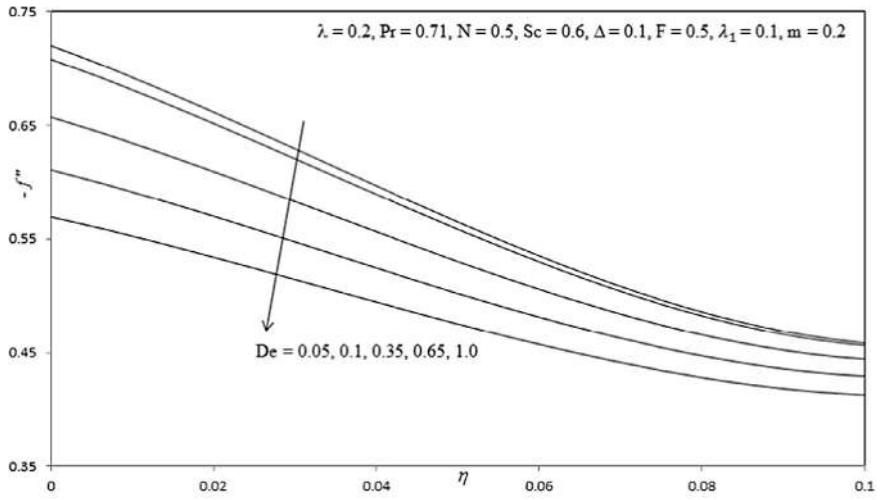

(a) Influence of De on Local Skin Friction Coefficient

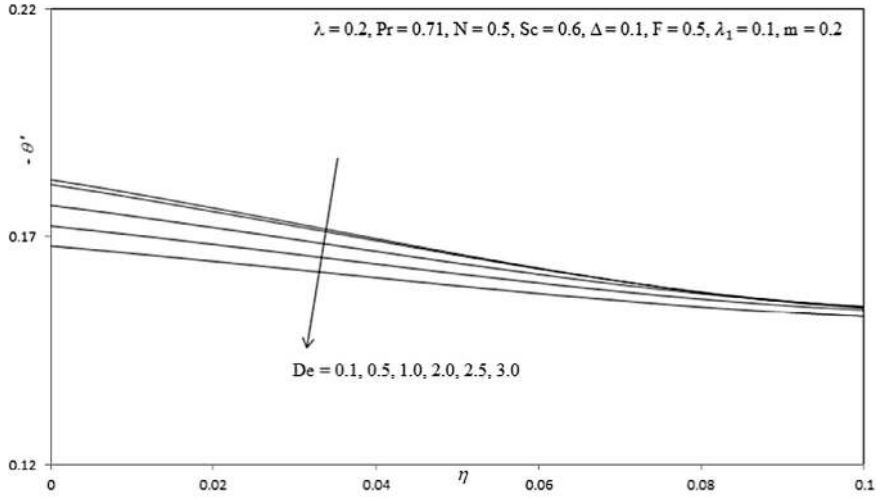

(b) Influence of De on Nusselt Number

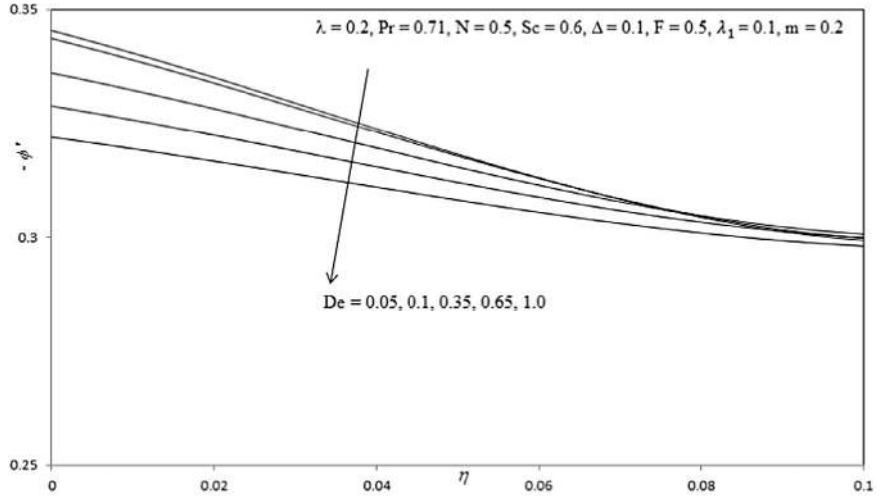

(c) Influence of De on Sherood Number

Figure 9 (a) Influence of *De* on local skin friction coefficient. (b) Influence of *De* on Nusselt number. (c) Influence of *De* on Sherwood number.

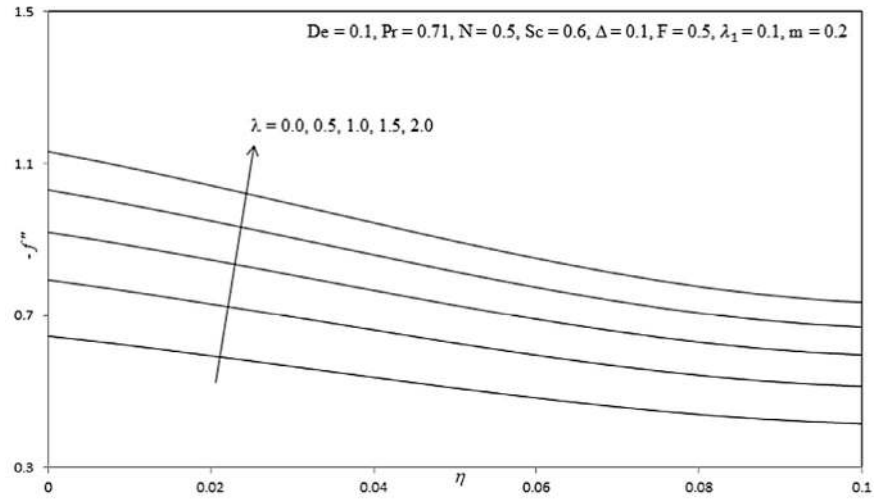

(a) Influence of λ on Local Skin Friction Coefficient

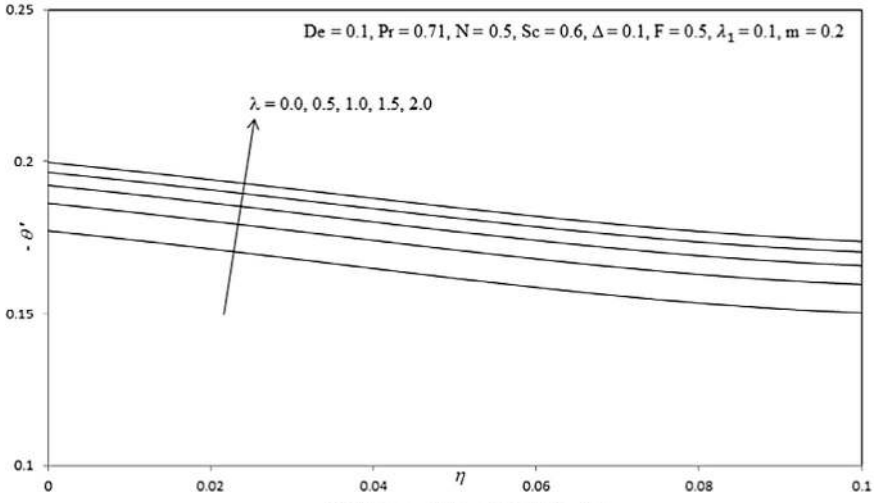

(b) Influence of λ on Nusselt Number

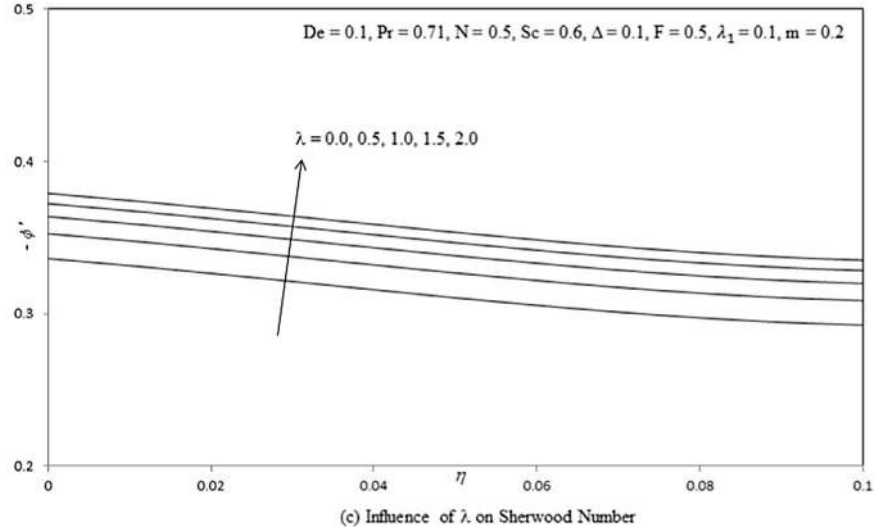

(c) Influence of λ on Sherwood Number

Figure 10 (a) Influence of λ on local skin friction coefficient. (b) Influence of λ on Nusselt number. (c) Influence of λ on Sherwood number.

5. Conclusions

A mathematical model has been developed for the non-similar, buoyancy-driven boundary layer mixed convection flow, heat and mass transfer of Jeffrey's non-Newtonian fluid from a non-isothermal wedge, in the presence of thermal radiation and heat generation/absorption. The transformed conservation equations have been solved with prescribed boundary conditions using the implicit finite difference Keller-Box method. A comprehensive assessment of the effects of De, λ, F, λ_1, Δ and N. Very accurate and stable results are obtained with the present finite difference code. The numerical code is able to solve nonlinear boundary layer equations very efficiently and therefore shows excellent promise in simulating transport phenomena in other non-Newtonian fluids. It is therefore presently being employed to study micropolar fluids and viscoplastic fluids which also represent other chemical engineering working fluids. The present study has neglected time effects. Future simulations will also address transient polymeric boundary layer flows and will be presented soon.

References

[1] Anwar Bég O, Abdel Malleque K, Islam MN. Modelling of Ostwald-deWaele non-Newtonian flow over a rotating disk in a non-Darcian porous medium. Int J Appl Math Mech 2012;8:46–67.

[2] Gouse Mohiddin S, Prasad VR, Anwar Bég O. Numerical study of unsteady free convective heat and mass transfer in a Walters-B viscoelastic flow along a vertical cone. Int J Appl Math Mech 2010;6:88–114.

[3] Prasad VR, Vasu B, Anwar Bég O, Parshad R. Unsteady free convection heat and mass transfer in a Walters-B viscoelastic flow past a semi-infinite vertical plate: a numerical study. Therm Sci-Int Sci J 2011;15(2):S291–305.

[4] Tripathi D, Anwar Bég O, Curiel-Sosa J. Homotopy semi-numerical simulation of peristaltic flow of generalized Oldroyd-B fluids with slip effects. Comput Methods Biomech Biomed Eng 2012. http://dx.doi.org/10.1080/10255842.2012.688109.

[5] Anwar Bég O, Takhar HS, Bharagava R, Rawat S, Prasad VR. Numerical study of heat transfer of a third grade viscoelastic fluid in non-Darcian porous media with thermophysical effects. Phys Scr 2008;77:1–11.

[6] Rashidi MM, Anwar Bég O, Rastegari MT. A study of non-Newtonian flow and heat transfer over a non-isothermal wedge using the homotopy analysis method. Chem Eng Commun 2012;199:231–56.

[7] Huilgol RR, You Z. Application of the augmented Lagrangian method to steady pipe flows of Bingham, Casson and Herschel–Bulkley fluids. J Non-Newton Fluid Mech 2005;128:126–43.

[8] Prasad V Ramachandra, Gaffar S Abdul, Keshava Reddy E, Anwar Bég O. Computational study of non-Newtonian thermal convection from a vertical porous plate in a non-Darcy porous medium with Biot number effects. J Porous Media 2014;17:601–22.

[9] Jeffreys H. The earth. 4th ed. London: Cambridge University Press; 1929.

[10] Bird RB, Armstrong RC, Hassager O. Dynamics of polymeric liquids. Fluid dynamics, 2nd ed., vol. 1. Wiley; 1987.

[11] Kothandapani M, Srinivas S. Peristaltic transport of a Jeffery fluid under the effect of magnetic field in an asymmetric channel. Int J Nonlinear Mech 2008;43:915–24.

[12] Nadeem S, Akbar NS. Peristaltic flow of a Jeffery fluid with variable viscosity in an asymmetric channel. Z Naturforsch A 2009;64a:713–22.

[13] Hayat T, Shehzad SA, Qasim M, Obaidat S. Radiative flow of Jeffery fluid in a porous medium with power law heat flux and heat source. Nucl Eng Des 2012;243:15–9.

[14] Prasad V Ramachandra, Gaffar S Abdul, Keshava Reddy E, Anwar Bég O. flow and heat transfer of Jeffrey's non-Newtonian fluid from horizontal circular cylinder. J Thermophys Heat Transfer 2014;28(4):764–70.

[15] Shehzad SA, Alsaedi A, Hayat T. Three-dimensional flow of Jeffrey fluid with convective surface boundary conditions. Int J Heat Mass Transfer 2012;55:3971–6.

[16] Prasad VR, Gaffar S Abdul, Keshava Reddy E, Anwar Bég O. Numerical study of non-Newtonian boundary layer flow of Jeffreys fluid past a vertical porous plate in a Non-Darcy porous medium. Int J Comput Methods Eng Sci Mech 2014;15(4):372–89.

[17] Ara Asmat, Khan Najeeb Alam, Khan Hassam, Sultan Faqiha. Radiation effects on boundary layer flow of an Eyring–Powell fluid over an exponentially shrinking sheet. Ain Shams Eng J 2014;5:1337–42.

[18] Noor NF, Abbasbandy S, Hashim I. Heat and mass transfer of thermophoretic MHD flow over an inclined radiate isothermal permeable surface in the presence of heat source/sink. Int J Heat Mass Transfer 2012;5:2122–8.

[19] Gupta D, Kumar L, Bég OA, Singh B. Finite element simulation of mixed convection flow of micropolar fluid over a shrinking sheet with thermal radiation. Proc IChemE-Part E, J Process Mech Eng 2012.

[20] Cortell R. Suction, viscous heating and thermal radiation effects on the flow and heat transfer of a power-law fluid past an infinite porous plate. Proc IChemE, Chem Eng Res Des 2011;89:85–93.

[21] Bhargava R, Sharma R, Bég OA. A numerical solution for the effect of radiation on micropolar flow and heat transfer past a horizontal stretching sheet through a porous medium. In: 7th SWEAS int conf on heat mass transfer (HMT'10). UK: University of Cambridge; 2010. p. 88–96.

[22] Rosenhead L. Laminar boundary layers. UK: Oxford; 1963.

[23] Cebeci T, Keller HB. Shooting and parallel shooting methods for solving the Falkner–Skan boundary-layer equation. J Comput Phys 1971;7:289–300.

[24] Peddieson J. Wedge and cone flows of viscoelastic liquids. AIChE J 1973;19:377–9.

[25] Sparrow EM, Eichhorn R, Gregg JL. Combined forced and free convection in boundary layer flow. Phys Fluids 1959;2:319–28.

[26] Watanabe T, Funazaki K, Taniguchi H. Theoretical analysis on mixed convection boundary layer flow over a wedge with uniform suction or injection. Acta Mech 1994;105:133–41.

[27] Kafoussias NG, Nanousis ND. Magnetohydrodynamic laminar boundary layer flow over a wedge with suction or injection. Can J Phys 1997;75:733–42.

[28] Nanousis ND. Theoretical magneto hydrodynamics analysis of mixed convection boundary layer flow over a wedge with uniform suction or injection. Acta Mech 1999;138:21–30.

[29] Gorla RSR. Unsteady heat transfer in laminar non-Newtonian boundary layer over a wedge. AIChemE J 1982;28:56–60.

[30] Yih KA. Radiation effects on mixed convection over an isothermal wedge in the porous media: the entire regime. Heat Transfer Eng 2001;22:26–32.

[31] Rashidi MM, Rastegari MT, Asadi M, Anwar Bég O. A study of non-Newtonian flow and heat transfer over a non-isothermal wedge using the homotopy analysis method. Chem Eng Commun 2012;199:231–56.

[32] Chamkha AJ, Mujtaba M, Quadri A, Issa C. Thermal radiation effects on MHD forced convection flow adjacent to a non-isothermal wedge in the presence of a heat source or sink. Heat Mass Transfer 2003;39:305–12.
[33] Hsiao K-L. MHD mixed convection for viscoelastic fluid past a porous wedge. Int J Non-Linear Mech 2011;46:1–8.
[34] Ishak A, Nazar R, Pop I. Moving wedge and flat plate in a micropolar fluid. Int J Eng Sci 2006;44(18–19):1225–36.
[35] Ishak A, Nazar R, Pop I. Moving wedge and flat plate in a power law fluid. Int J Non-Linear Mech 2011;46(8):1017–21.
[36] Ishak A, Nazar R, Pop Ioan. MHD boundary-layer flow of a micropolar fluid past a wedge with constant wall heat flux. Commun Nonlinear Sci Numer Simul 2009;14(1):109–18. http://dx.doi.org/10.1016/j.cnsns.2007.07.011.
[37] Ishak A, Nazar R, Pop Ioan. MHD boundary-layer flow of a micropolar fluid past a wedge with variable wall temperature. Acta Mech 2008;196(1–2):75–86. http://dx.doi.org/10.1016/j.cnsns.2007.07.011.
[38] Sturdza P. An aerodynamic design method for supersonic natural laminar flow aircraft. PhD thesis. Dept. Aeronautics and Astronautics, Stanford University, California, USA; December 2003.
[39] Bird RB, Armstrong RC, Hassager O. Dynamics of polymeric liquids. Fluid mechanics, vol. 1. New York: Wiley; 1977.
[40] Gorla RSR. Radiative effect on conjugate forced convection in a laminar wall jet along a flat plate. Encyclopedia fluid mechanics. Advances in flows dynamics. Texas (USA): Gulf Publishing; 1993 (Suppl. 3).
[41] Anwar Bég O, Zueco J, Ghosh SK, Heidari A. Unsteady magnetohydrodynamic heat transfer in a semi-infinite porous medium with thermal radiation flux: analytical and numerical study. Adv Numer Anal 2011;2011:1–17.
[42] Keller HB. Numerical methods in boundary-layer theory. Ann Rev Fluid Mech 1978;10:417–33.
[43] Anwar Bég O. Numerical methods for multi-physical magnetohydrodynamics. In: New developments in hydrodynamics research. New York: Nova Science; 2012. p. 1–112 [Chapter 1].
[44] Lok YY, Pop I, Ingham DB. Oblique stagnation slip flow of a micropolar fluid. Meccanica 2010;45:187–98.
[45] Chang T-B, Mehmood A, Anwar Bég O, Narahari M, Islam MN, Ameen F. Numerical study of transient free convective mass transfer in a Walters-B viscoelastic flow with wall suction. Commun Nonlinear Sci Numer Simul 2011;16:216–25.
[46] Srinivasacharya D, Kaladhar K. Mixed convection flow of couple stress fluid in a non-Darcy porous medium with Soret and Dufour effects. J Appl Sci Eng 2012;15:415–22.
[47] Gaffar S Abdul, Prasad V Ramachandra, Anwar Bég O. Computational analysis of magnetohydrodynamic free convection flow and heat transfer of non-Newtonian tangent hyperbolic fluid from a horizontal circular cylinder with partial slip. Int J Appl Comput Math 2015:25. http://dx.doi.org/10.1007/s40819-015-0042-x.
[48] Prasad VR, Gaffar SA, Anwar Bég O. Heat and mass transfer of a nanofluid from a horizontal cylinder to a micropolar fluid. AIAA J Thermophys Heat Transfer 2015;29:127–39.
[49] Darji RM, Timol MG. On invariance analysis of MHD boundary layer equations for non-Newtonian Williamson fluids. Int J Adv Appl Math Mech 2014;1:10–9.
[50] Singh V, Agarwal S. Flow and heat transfer of Maxwell fluid with variable viscosity and thermal conductivity over an exponentially stretching sheet. Am J Fluid Dyn 2013;3:87–95. http://dx.doi.org/10.5923/j.ajfd.20130304.01.
[51] Minkowycz WJ, Sparrow EM, Schneider GE, Pletcher RH. Handbook of numerical heat transfer. New York: John Wiley and Sons; 1988.

S. Abdul Gaffar was born in Madanapalle, Chittoor District, Andhra Pradesh, India, in May, 1982. He completed a First Class Masters of Sciences, degree in Mathematics (2004) from Sri Venkateswara University, Tirupati, and is pursuing PhD in Flow and Heat transfer of Casson Fluid on Boundary Layer (Registered in 2011), JNT University Anantapur, Anantapuramu. He worked as lecturer in the Department of Mathematics, Bapatla College of Engineering, India, for one year (2004). Later from May 2007 to April 2013, he was the Assistant Professor for five years in the Department of Mathematics, Mother Theresa Institutions. From 2013 to till date he is working as Lecturer in the Department of Mathematics, Salalah college of Technology, Salalah, Oman. He has published in excess of 14 journals in peer reviewed journals. He is currently engaged in different non-Newtonian fluids over different curved bodies.

Professor Dr. V. Ramachandra Prasad was born in Madanapalle, Chittoor District, Andhra Pradesh, India, in July, 1968. He completed a Distinction Class Masters of Sciences, degree in Mathematics (1994) from Osmania University, Hyderabad, and a PhD in Radiation and Mass Transfer Effects on connective flow past a vertical plate (2003), both from Sri Venkateswara University, Tirupati. He then worked as lecturer in the Department of Mathematics, Besant Theosophical College, Madanapalle, India, for seven years (1994–2001). From May 2001 to April 2007, he was the Assistant Professor for six years in the Department of Mathematics, in Madanapalle Institute of Technology and Science. Later from May 2007 to April 2009 worked as Associate Professor, in the Department of Mathematics, Madanapalle Institute of Technology and Science, Madanapalle, India. From May 2009 to till date he is working as Professor in the Department of Mathematics, Madanapalle Institute of Technology and Science, Madanapalle, India. He has authored Radiation effects on Convective Flow Past a Vertical Plate: Radiation and Mass Transfer Effects on Convective Flow Past a Vertical Plate (Lambert, Germany, 2010), Thermo-Diffusion and Diffusion-Thermo Effects on Boundary Layer Flows (*Lambert, Germany, 2011) and Walters_B Viscoelastic flow Past a Vertical Plate: Numerical Study of Unsteady Free Convective Heat and Mass Transfer in a Walters_B Viscoelastic Flow Past a Vertical Plate (Lambert, Germany, 2012*). He has published in excess of 50 journal articles. His research has also been presented at over 13 conferences. He is currently engaged in different non-Newtonian fluids over different curved bodies.

Dr. E. Keshava Reddy, presently working as Professor of Mathematics in JNT University College of Engineering Anantapur. He has 15 years of experience in teaching and 11 years in research. He completed his PhD degree in Mathematics from prestigious University Banaras Hindu University Varanasi. His areas of interest include Functional Analysis, Optimization Techniques, Data Mining, Neural Networks, Fuzzy Logic and Optimization techniques. He guided 2 PhD, 1 MPhil and has published more than 35 Research papers in National and International Journals and Conferences. He authored 06 books on Engineering Mathematics and Mathematical Methods for various universities. He worked as Chairman of Board of studies for the faculty of Mathematics for JNTUA both at UG level and at PG level. Presently he is the chairman, PG Board of studies for Mathematics of JNTUA. He is a member of Board of Studies for Mathematics of various universities.